

# A Novel Approach to Productivity Prediction of Carbonate Gas Reservoirs from Electrical Image Logs\*

Bing Xie<sup>1</sup>, Fu-Sen Xiao<sup>1</sup>, Qiang Lai<sup>1</sup>, Yu-Yu Wu<sup>1</sup>, and Da-Li Wang<sup>2</sup>

Search and Discovery Article #42277 (2018)\*\*

Posted September 24, 2018

\*Adapted from extended abstract prepared in conjunction with poster presentation given at AAPG 2018 AAPG Annual Convention and Exhibition, Salt Lake City, Utah, May 20-23, 2018

\*\*Datapages © 2018 Serial rights given by author. For all other rights contact author directly. DOI:10.1306/42277Xie2018

<sup>1</sup>PetroChina SWOGC, Chengdu, China ([xxb-th@petrochina.com.cn](mailto:xxb-th@petrochina.com.cn))

<sup>2</sup>DCS, Schlumberger, Chengdu, China ([DWang7@slb.com](mailto:DWang7@slb.com))

## Abstract

The production rate data and electrical image logs from 23 wells were used to set up an artificial neural network (ANN) model for the productivity prediction of carbonate gas reservoirs. The inputs of the ANN model are the attributes of weathering dissolution vugs, including connectedness, surface proportion, size, and thickness of vug zones. The ANN model was used to predict the gas production rates in two new wells. The predicted gas production rates separately are  $70 \times 10^4 \text{ m}^3/\text{d}$  and  $200 \times 10^4 \text{ m}^3/\text{d}$ , and the actual gas production rates are  $101.97 \times 10^4 \text{ m}^3/\text{d}$  and  $182 \times 10^4 \text{ m}^3/\text{d}$ . The approach provided satisfactory results.

The poor regression relationship between the conventional open hole logs and production rate motivated maximizing the use of electrical image logs, which provide details of the pore space of the reservoirs. Core observation and core laboratory analysis indicate that the pore space of the carbonate gas reservoirs mainly consists of vugs and fractures. Most of the fractures are weathered fractures with high angle, which are well-developed almost everywhere. The horizontal well trajectories perpendicular to northwest/southeast direction cut through more fractures, whereas the horizontal well trajectories parallel to northwest/southeast direction drill through fewer fractures. The vugs, however, are randomly distributed both laterally and vertically. This represents a complex heterogeneous carbonate reservoir in which the vugs are a key contributor to the total pore space of the carbonate gas reservoir.

Accurately identifying and quantifying the pore space of vugs is critical to the productivity prediction of the carbonate gas reservoirs. Typically, it is very difficult to use open hole logs to identify vugs because artificial drilling events and vugs have similar open hole log responses. However, high-resolution electrical image logs are sensitive to the different types of vugs, such as connected vugs, isolated vugs, etc. With the help of the advanced processing techniques of the electrical images, it is possible to extract quantitative measures of important reservoir parameters from the electrical image logs. The connectedness of vugs serves as the permeability index, the surface area of vugs serves as the porosity index, and the size of vugs is vug density. The electrical image logs are thus used to delineate heterogeneous porosity and permeability of the carbonate gas reservoirs.

The case study demonstrates the quantification of the pore space of vugs from electrical image logs and the productivity prediction of carbonate gas reservoirs by the ANN model and presents the relationship between well trajectory and natural fractures. In addition, the case study indicates that neural network modeling is a good solution for the establishment of the complex multivariable relationships between the attributes of vugs and gas production rates, and such modeling can be used for productivity prediction of the carbonate gas reservoirs. The lessons learned from this case study suggest that the borehole wall coverage of electrical images impacts the quantification of vug attributes and the productivity prediction. Analysis of high-resolution logging-while-drilling (LWD) image logs with full borehole coverage would further improve the technique.

## **Introduction**

Carbonate gas reservoirs from the Dengying Formation formed in the late Precambrian marine carbonate depositional environments of platform margin and mound shoal (Zou et al., 2014). The Dengying Formation is primarily dolomite, which is mainly algal dolomite and crystalline dolomite, with occasional saddle dolomite. A long period of weathering and erosion formed karst features including locally well-developed dissolution vugs and caves in the Dengying Formation. However, a long period of deep burial and diagenesis occluded porosity (Shi et al., 2013). Particularly, the materials formed from burial-hydrothermal process filled the porosity (Chen et al., 2017). The carbonate reservoir porosity of the Dengying Formation is predominantly from dissolution vugs. The average porosity of the reservoirs is 2.2% to 3.9%, and the average permeability is 0.59 md (Wei et al., 2015).

The pore space of vugs in the Dengying Formation is very complex due to the formation's spatial heterogeneity and the partially/fully filled vugs that decrease the porosity and permeability of the pore space. Conventional logs fail to identify the partially and fully filled vugs. The presence of partially and fully filled vugs is one of the main reasons for the poor regression relationship between conventional open hole logs and gas production rate in the Dengying Formation.

The case study in this paper reveals that the vug properties from electrical image logs, i.e., vug connectedness, vug surface proportion, and vug size, correspond to the reservoir quality of the pore space of vugs and the gas production performance in the Dengying Formation. The vug properties represent and quantify the varying degrees of partially and fully filled vugs.

## **Log Responses in Gas Perforation Interval**

The gas production performance in the 23 wells suggests that vertical wells could have higher gas production rate than horizontal wells, such as in well 2, well 3, and well 18 (Table 1). The gas production rates, however, are very different, even among vertical wells, as shown in Figure 1. From conventional logs, it is difficult to identify the difference of the log responses in the gas perforation intervals. For example, Figure 2 shows three-well composite plots, including well 12, well 16, and well 18. The porosities from the conventional logs are nearly the same among the perforation intervals (on track 9 in Figure 2), but the gas production rates in the perforation intervals are very different.

The vug properties, such as connectedness, surface proportion, and size, were extracted from the electrical image logs by image processing techniques (Wang and Xie, 2017). It is clear that the vug properties among the perforation intervals of the three wells are very different (Figure 2).

### **Natural Fracture versus Gas Production Rate**

The natural high-angle fractures were interpreted from the electrical image logs in 10 of the 23 wells, as shown in Figure 3. Most of the fracture strikes are northwest/southeast; a few fractures strike toward the northeast/southwest. Figure 3 and Figure 4 indicate that the number of the fractures could depend on well trajectory in deviated wells and horizontal wells; the well trajectories perpendicular to northwest/southeast direction drill through more fractures than the wells parallel to northwest-southeast direction. This suggests that the fractures could be well-developed almost everywhere.

The gas production rates and the fracture interpretation results indicate that the fractures are not the primary factor in gas production performance; examples are well 2 and well 23 (Table 1). It suggests that unfilled dissolution vugs could be the main factor to gas production in the Dengying Formation.

### **Vug Properties versus Gas Production Rate**

The vug properties from the electrical image logs include vug connectedness, vug surface proportion, and vug size, as well as cumulative thickness of vug zones. The vug connectedness can be used as a permeability indicator, the vug surface proportion can be used as a porosity indicator, and vug size can be used as a vug density indicator.

Figure 5 indicates that the relationship between gas production rate and each of the vug properties seems like a quadratic function and/or a linear function, particularly if the vug property is greater than a threshold (indicated by the red triangle on the x-axis in the crossplots). The porosity from conventional logs, however, has no function relationship with the gas production rate (Figure 6). But it is clear that the relationship between the vug properties and gas production rates cannot be expressed in the form of an explicit function.

### **ANN Model for Gas Productivity Prediction**

The ANN model in the case study is a four-layer neural network, including input layer, two middle layers, and output layer, as shown in Figure 7. The nodes of the input layer consist of the vug properties, including connectedness, surface proportion, size, and thickness of vug zones. The node of the output layer is gas production rate. The nodes of the two middle layers remain the network weights that are calculated from a training data set. The network weights represent the relationship between the vug properties and gas production rates in the form of an implicit function.

The training of the ANN model comprises the following steps:

- Initialize the node weights.

- Input samples one by one from the training data set and calculate the node weights.
- Adjust the weights if the error difference from the output node is not satisfied and repeat steps 2 and 3 until the weights are stable and the network is converged.

The training data set is from the 23 wells, as shown in [Table 2](#). Well 4 and well 5 each had two gas production tests, one in the upper section (-U) and one in the lower section (-L).

After the ANN model has been trained, it can be used to predict gas production rate. The vug properties are input from the electrical image logs, and the output is the predicted gas production rate.

The ANN model was used to predict the gas production rates in two new wells in the case study. The predicted gas production rates separately are  $70 \times 10^4 \text{ m}^3/\text{d}$  and  $200 \times 10^4 \text{ m}^3/\text{d}$ , and the actual gas production rates are  $101.97 \times 10^4 \text{ m}^3/\text{d}$  and  $182 \times 10^4 \text{ m}^3/\text{d}$ . The ANN model provided satisfactory results.

### Conclusions

High-resolution electrical image logs make determining vug properties possible. The vug properties reflect the reservoir quality of the pore space in the Dengying Formation.

The presence of natural fractures is not the primary factor in gas production performance. Vugs are the main factor in gas production in the Dengying Formation.

An artificial neural network (ANN) can represent the complex relationship between the vug properties and gas production rates in the form of an implicit function.

### Acknowledgments

The authors would like to thank PetroChina SWOGC for supporting the electrical image log data acquisition. We also thank PetroChina SWOGC Institute for permission to publish the paper and release the data.

### References Cited

Chen, Y.N., A.J. Shen, L.Y. Pan, J. Zhang, and X.F. Wang, 2017, Features, Origin, and Distribution of Microbial Dolomite Reservoirs: A Case Study of the 4th Member of Sinian Dengying Formation in Sichuan Basin, SW China: *Petroleum Exploration and Development*, v. 44/5, p. 704-715. doi.org/10.1016/s1876-3804(17)30085-x

Shi, Z.J., Y. Wang, Y.M. Tian, and C.C. Wang, 2013, Cementation and Diagenetic Fluid of Algal Dolomites in the Sinian Dengying Formation in Southeastern Sichuan Basin: *Science China Earth Science*, v. 43.2, p. 317-328. doi.org/10.1007/s11430-012-4541-x

Wang, D.L. and B. Xie, 2017, Permeability Index of Vugs and Fractures in Heterogeneous Carbonate Gas Reservoirs from High-Resolution Electrical Images: Presented at APGCE 2017 Asia Petroleum Geoscience Conference & Exhibition, Kuala Lumpur, Malaysia, 20–21 November, oral presentation 43114 in Session 21: Carbonates.

Wei, G.Q., W. Yang, J.H. Du, C. Xu, C. Zou, W. Xie, S. Wu, and F. Zeng, 2015, Tectonic Features of Gaoshiti-Moxi Paleo-Uplift and its Controls on the Formation of a Giant Gas Field, Sichuan Basin, SW China: *Petroleum Exploration and Development*, v. 42/3, p. 257-265. doi.org/10.1016/s1876-3804(15)30018-5

Zou, C.N., J.H. Du, C.C. Xu, Z. Wang, B. Zhang, G. Wei, T. Wang, G. Yao, S. Deng, J. Liu, H. Zhou, A. Xu, Z. Yang, H. Jiang, and Z. Gu, 2014, Formation, Distribution, Resource Potential, and Discovery of the Sinian-Cambrian Giant Gas Field, Sichuan Basin, SW China: *Petroleum Exploration and Development*, v. 41/3, p. 278-293. doi.org/10.1016/s1876-3804(14)60036-7

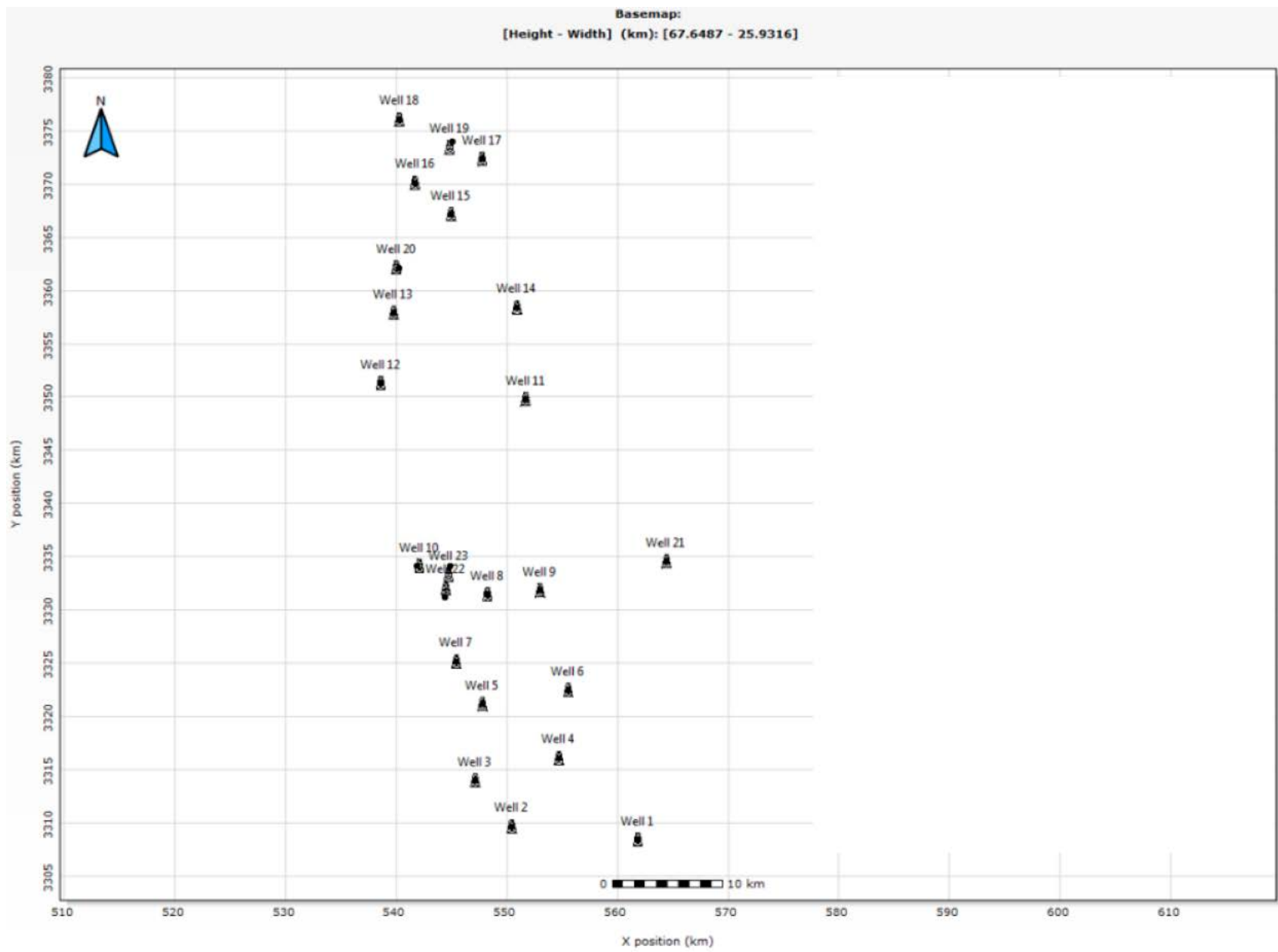


Figure 1. Well location map and gas production table.

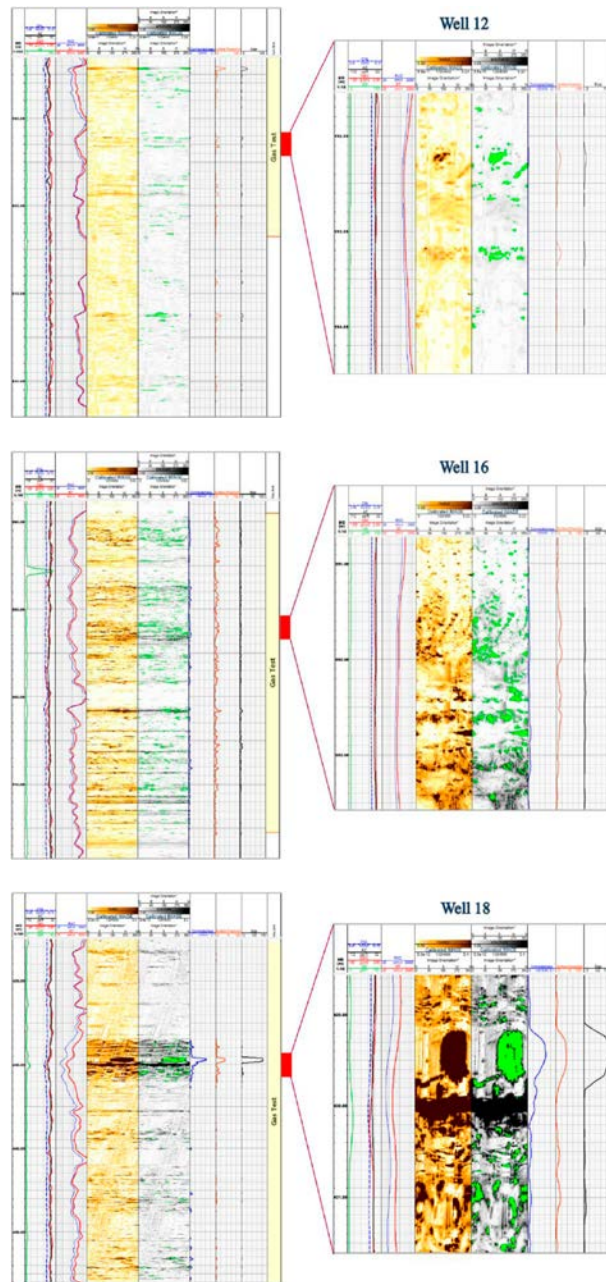


Figure 2. Three-well composite plots associated with the vug properties: connectedness in track 6, surface proportion in track 7, and size in track 8. Neutron log (CNL), density log (DEN), sonic log (AC), and gamma ray log (GR) are shown in track 2; shallow and deep resistivity logs in track 3; and calibrated image in track 4. The extracted unfilled-vug image is in track 5.

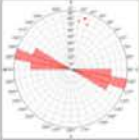

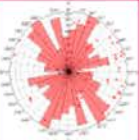

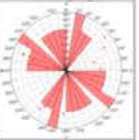

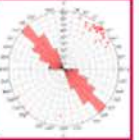
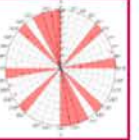
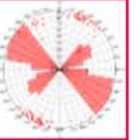
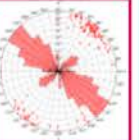


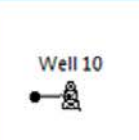







	Well 5	Well 7	Well 10	Well 15	Well 16	Well 18	Well 19	Well 20	Well 22	Well 23
Number of Fracture	4	2	48	3	14	12	37	9	107	122
Fracture Strike Rosette										
Well Trajectory Direction	 D	 V	 D	 V	 V	 V	 D	 D	 D	 H

Figure 3. Fracture interpretation results from the electrical image logs, associated with well trajectory directions. D, V, and H stand for deviated well, vertical well, and horizontal well, respectively.



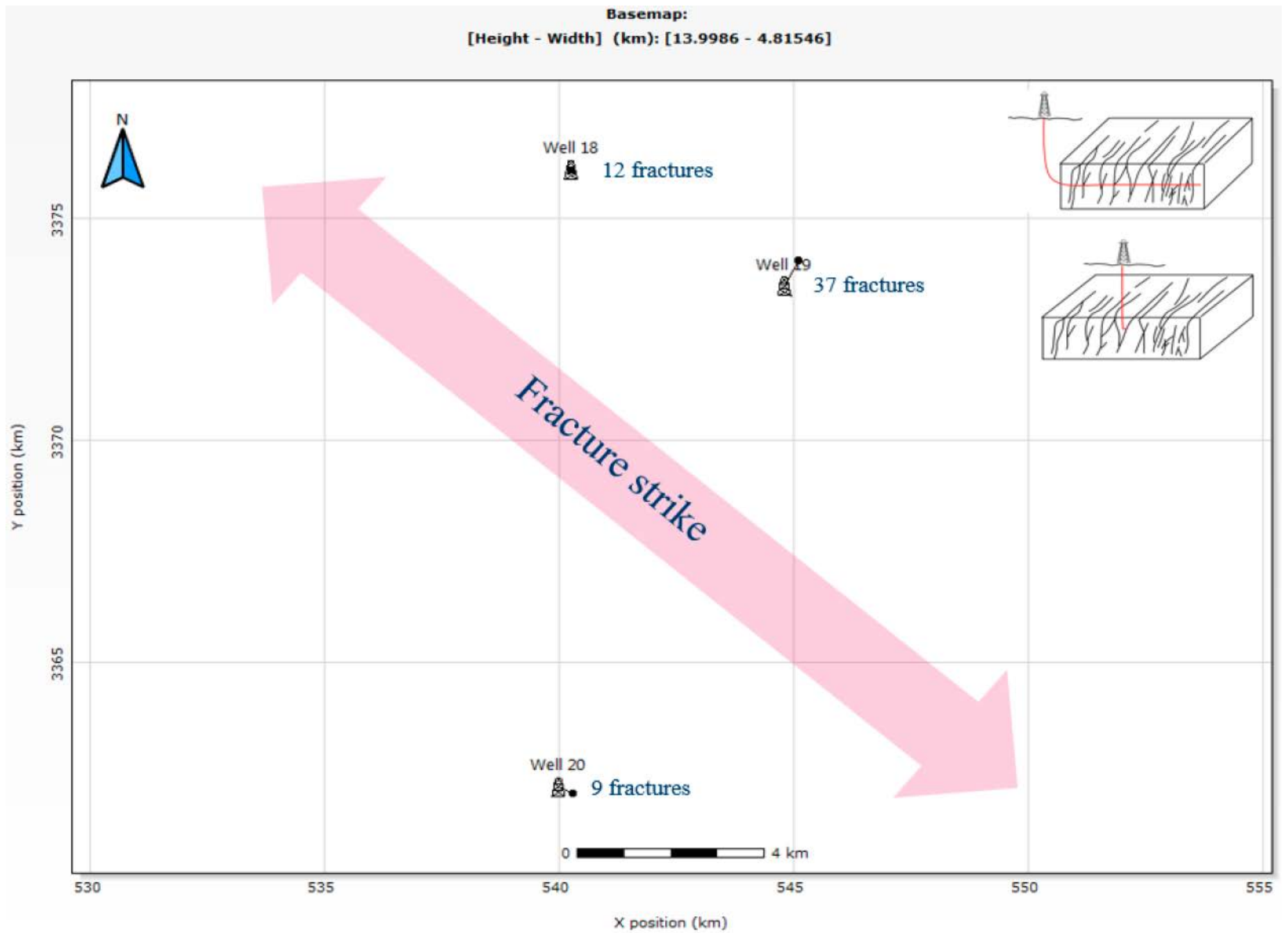


Figure 4. The relationship between fracture strike and well trajectory direction.

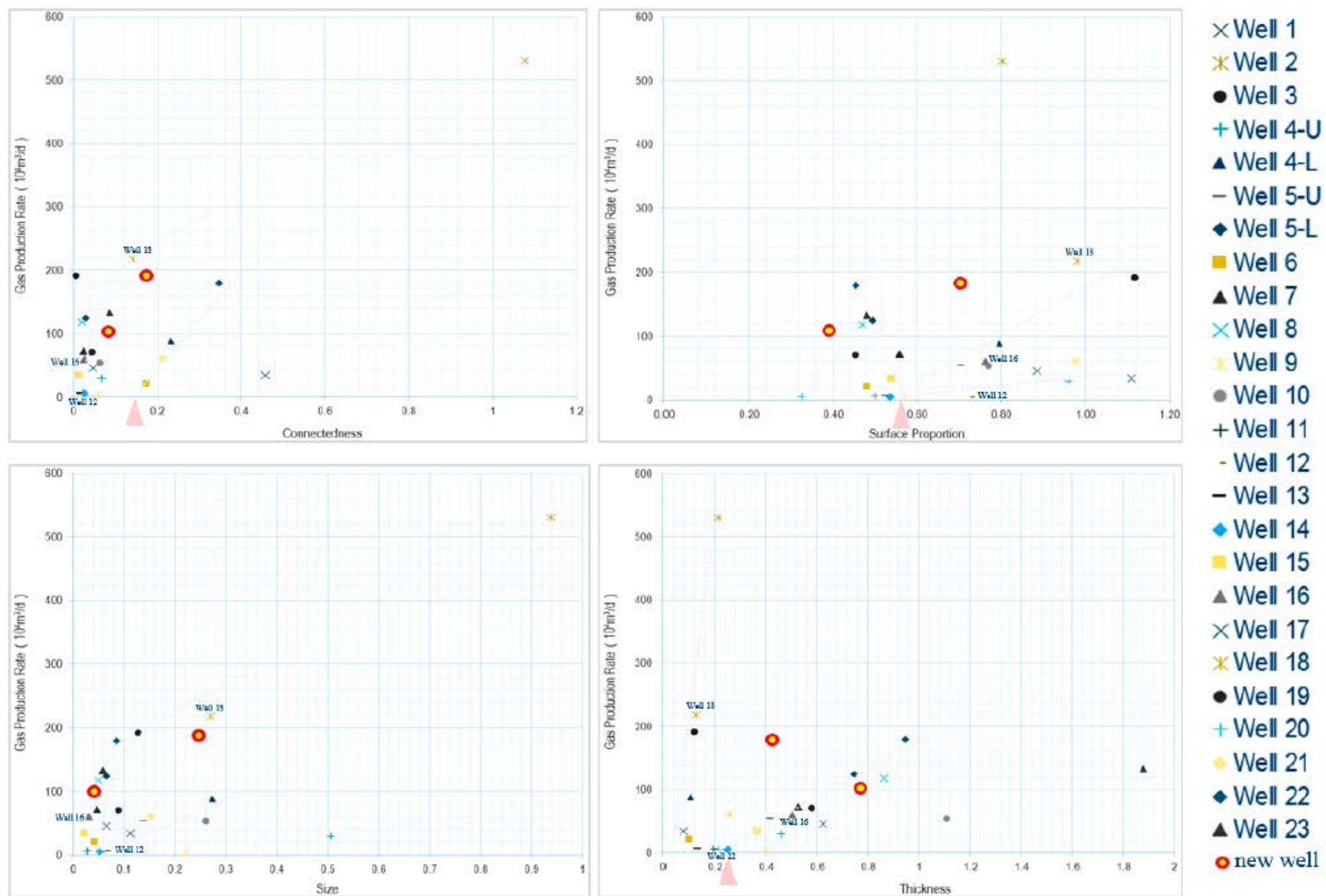


Figure 5. Crossplot of the gas production rate and the vug properties from the electrical image logs in 25 wells.

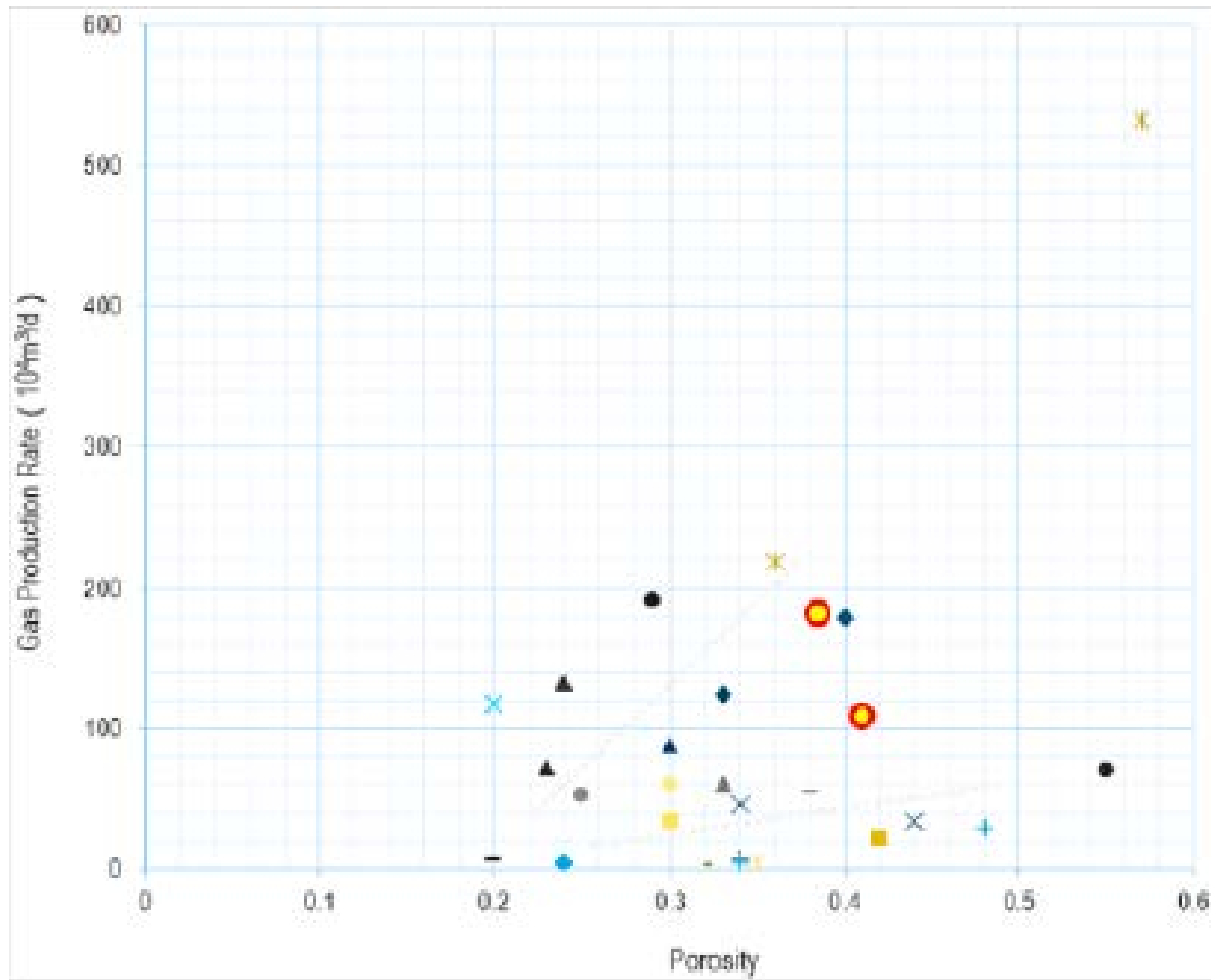


Figure 6. Crossplot of the gas production rate and the porosity from the conventional logs in 25 wells.

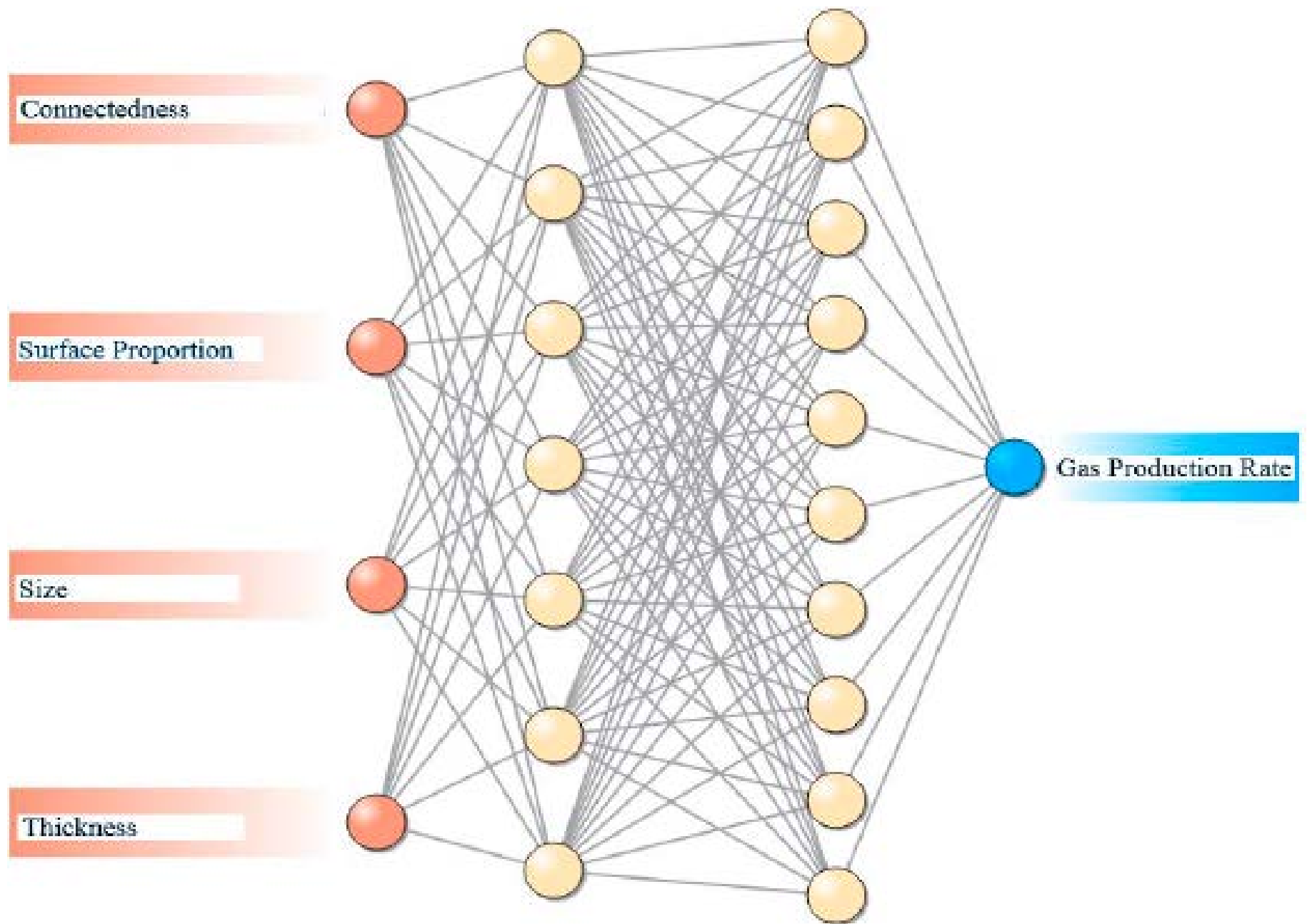


Figure 7. Productivity prediction model of artificial neural networks.

<b>Well Name</b>	<b>Gas Production Rate (10<sup>4</sup> m<sup>3</sup>/day)</b>	<b>Well Geometry</b>
Well 1	33.95	vertical well
Well 2	531.01	vertical well
Well 3	190.53	vertical well
Well 4	117.54	deviated well
Well 5	178.49	deviated well
Well 6	21.50	vertical well
Well 7	71.83	vertical well
Well 8	117.40	deviated well
Well 9	4.24	vertical well
Well 10	53.02	deviated well
Well 11	6.49	vertical well
Well 12	3.48	vertical well
Well 13	6.35	vertical well
Well 14	4.71	vertical well
Well 15	33.95	vertical well
Well 16	60.00	vertical well
Well 17	45.51	vertical well
Well 18	217.58	vertical well
Well 19	69.78	deviated well
Well 20	4.69	deviated well
Well 21	60.60	vertical well
Well 22	179.11	deviated well
Well 23	132.37	horizontal well

Table 1. Production test data of the 23 wells.

Well Name	Connectedness	Surface Proportion	Size	Thickness	Gas Production Rate (10 <sup>4</sup> m <sup>3</sup> /day)
Well 1	0.458	1.108	0.112	0.076	33.95
Well 2	1.079	0.802	0.938	0.213	531.01
Well 3	0.006	1.118	0.129	0.119	190.53
Well 4-U	0.067	0.960	0.506	0.458	29.87
Well 4-L	0.233	0.795	0.274	0.106	87.67
Well 5-U	0.026	0.703	0.138	0.416	54.30
Well 5-L	0.029	0.494	0.065	0.744	124.19
Well 6	0.174	0.479	0.043	0.100	21.50
Well 7	0.023	0.557	0.046	0.524	71.83
Well 8	0.020	0.469	0.050	0.863	117.40
Well 9	0.060	0.569	0.222	0.399	4.24
Well 10	0.063	0.771	0.261	1.109	53.02
Well 11	0.022	0.499	0.030	0.192	6.49
Well 12	0.010	0.729	0.056	0.193	3.48
Well 13	0.017	0.524	0.069	0.131	6.35
Well 14	0.027	0.535	0.051	0.248	4.71
Well 15	0.011	0.539	0.022	0.365	33.95
Well 16	0.025	0.760	0.031	0.501	60.00
Well 17	0.045	0.884	0.066	0.622	45.51
Well 18	0.141	0.981	0.269	0.126	217.58
Well 19	0.044	0.453	0.090	0.581	69.78
Well 20	0.028	0.325	0.023	0.214	4.69
Well 21	0.212	0.977	0.153	0.256	60.60
Well 22	0.347	0.454	0.086	0.944	179.11
Well 23	0.086	0.479	0.059	1.877	132.37

Table 2. Training data set after normalization preprocessing.